Solution Structure of a Brodimoprim Analogue in Its Complex with *Lactobacillus casei* Dihydrofolate Reductase†

William D. Morgan,‡ Berry Birdsall,‡ Vladimir I. Polshakov,‡,§ Daša Šali,‡ Ivan Kompis,|| and James Feeney*,‡

Laboratory of Molecular Structure, National Institute for Medical Research, Mill Hill, London NW7 1AA, U.K., and F. Hoffmann-La Roche Ltd., 4002 Basel, Switzerland

Received March 15, 1995; Revised Manuscript Received June 22, 1995⊗

ABSTRACT: Two-dimensional (2D) double-quantum-filtered correlation spectroscopy (DQF-COSY), total correlation spectroscopy (TOCSY), nuclear Overhauser effect spectroscopy (NOESY), and rotating-frame NOESY (ROESY) spectra were used to assign essentially all the protons in a 1:1 complex of *Lactobacillus casei* dihydrofolate reductase formed with an analogue of the antibacterial drug brodimoprim [2,4-diamino-5-(3′,5′-dimethoxy-4′-bromobenzyl)pyrimidine]. The analogue has a 4,6-dicarboxylic acid side chain substituted on the 3′-O position designed to interact with the Arg 57 and His 28 residues in *L. casei* dihydrofolate reductase; it binds a factor of 10^3 more tightly to the enzyme than does the parent compound. Thirty-eight intermolecular and 11 intramolecular NOEs were measured involving the bound brodimoprim-4,6-dicarboxylic acid analogue. These provided the distance constraints used in conjunction with an energy minimization and simulated annealing protocol (using Discover from Biosym Ltd.) to dock the brodimoprim analogue into dihydrofolate reductase. In calculations where side chains and backbone fragments for binding-site residues were allowed flexibility, 90% of the 40 calculated structures had reasonable covalent geometry and none of them had NOE distance violations of greater than 0.36 Å. The conformations of the aromatic rings in the bound ligand were well-defined in all the structures, with torsion angles $\tau_1 = -153° \pm 4°$ (C4−C5−C7−C1′) and $\tau_2 = 53° \pm 4°$ (C5−C7−C1′−C2′): the aromatic rings of the ligand occupied essentially the same space in all the calculated structures (root mean square deviation value 1.83 Å). Inclusion of the electrostatic interactions into the energy minimizations indicated that structures in which the 4,6-dicarboxylate group of the ligand interacts with the side chains of Arg 57 and His 28 are of low energy. Significant differences in side-chain and backbone conformations were detected between binding-site residues in the enzyme complexes with the brodimoprim analogue and methotrexate.

Trimethoprim [2,4-diamino-5-(3′,4′,5′-trimethoxybenzyl)-pyrimidine, **1**] is a clinically useful antibacterial drug which acts by selectively inhibiting the enzyme dihydrofolate reductase in bacterial cells (Blakley, 1985). A substantial amount of structural information has been obtained for complexes of trimethoprim with the enzyme[1] from X-ray crystallography and NMR spectroscopy [Baker *et al.*, 1981, 1982; Cayley *et al.*, 1979; Matthews *et al.*, 1985; Groom *et al.*, 1991; Martorell *et al.*, 1994 (and reviews: Blakley, 1985; Feeney, 1990)]. In the past, many trimethoprim analogues have been synthesized in attempts to find inhibitors which might have potential as improved antibacterial drugs (Roth & Cheng, 1982). For example, Kuyper *et al.* (1982) designed a series of trimethoprim analogues with aliphatic ω-carboxylic acid substituents arranged to interact favorably with a conserved Arg residue (Arg 57) in *Escherichia coli* dihydrofolate reductase and used X-ray crystallography to examine the complex formed with the enzyme. In concurrent studies, we prepared and examined a series of analogues of the related antibacterial drug brodimoprim [2,4-diamino-5-(3′,5′-dimethoxy-4′-bromobenzyl)pyrimidine, **2**] which had substituents at the 3′-O position designed to interact with this conserved arginine and also to make additional interactions with the protein (Birdsall *et al.*, 1984b). One of these (**3**) had a 4,6-dicarboxylic acid side chain designed to interact with Arg 57 and His 28 in *Lactobacillus casei* dihydrofolate reductase and this analogue was found to bind a factor of 10^3 more tightly to the enzyme than does the parent molecule, brodimoprim. The inhibition constant (K_i) for the dicarboxylic compound is <0.01 nM, compared to 11 nM for brodimoprim itself. Kompis and Then (1984) showed that this analogue **3** retains its high specificity for the bacterial enzyme, but it did not prove to be an effective antibacterial agent due to reduced membrane permeability. Early ^{1}H NMR studies, based largely on considerations of ^{1}H chemical shifts, were used to determine the bound conformations of the ligand and also to monitor its specific interactions with

† The coordinates of the dihydrofolate reductase−brodimoprim-4,6-dicarboxylate complex were deposited in the Brookhaven National Laboratory Protein Data Bank with the following ID codes: 1DIS for the minimized average structure, 1DIU for 18 docked structures, and R1DIUMR for the NMR restraints file.

* Author to whom correspondence should be addressed.

‡ National Institute for Medical Research.

§ Supported by a Wellcome Trust fellowship.

|| F. Hoffmann-La Roche Ltd.

⊗ Abstract published in *Advance ACS Abstracts,* August 15, 1995.

[1] Abbreviations: 2D, two-dimensional; BDM, brodimoprim; BDM-4,6, brodimoprim-4,6-dicarboxylate, systematic name 2-[3-[[6-bromo-α-(2,4-diamino-5-pyrimidinyl)-5-methoxy-*m*-tolyl]oxy]propyl]glutaric acid; COSY, two-dimensional correlation spectroscopy; DAP, 2,4-diaminopyrimidine; DANTE, delays alternating with nutation for tailored excitation; DHFR or enzyme, dihydrofolate reductase (EC 1.5.1.3); DQF-COSY, double-quantum-filtered correlation spectroscopy; DSS, sodium 2,2-dimethyl-2-silapentane-5-sulfonate; MTX, methotrexate; NOE, nuclear Overhauser effect; NOESY, two-dimensional nuclear Overhauser effect spectroscopy; ROE, rotating-frame nuclear Overhauser effect; ROESY, rotating-frame nuclear Overhauser effect spectroscopy; RMSD, root mean square deviations; TMP, trimethoprim; TOCSY, total correlation spectroscopy; SCUBA, stimulated cross-peaks under bleached alphas.

0006-2960/95/0434-11690$09.00/0

His 28. The overall conformation of the two rings in the bound analogue appeared to be similar in the enzyme complexes of trimethoprim, brodimoprim, and the brodimoprim-4,6-dicarboxylate analogue. In the complex with the 4,6-dicarboxylate analogue, the pK_a value of His 28 was increased by 1 unit compared to its value in the free enzyme (from 6.8 to 7.8). A similar increase had been detected earlier in all complexes formed with substrate analogues containing a glutamyl moiety such as methotrexate **4** (Birdsall *et al.*, 1977; Antonjuk *et al.*, 1984). In the crystal structure of the methotrexate−NADPH−DHFR complex (Bolin *et al.*, 1982), the γ-carboxylate group of the methotrexate glutamyl fragment is very close to the imidazole ring of His 28 and the change in pK_a of His 28 was interpreted as reflecting an ion−ion electrostatic interaction between the two groups. The similar increase in the pK_a of His 28 detected on forming the complex with the brodimoprim-4,6-dicarboxylate **3** suggested that one of the carboxylate groups is similarly interacting with His 28.

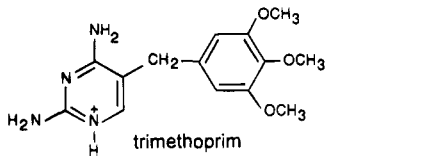

1 trimethoprim

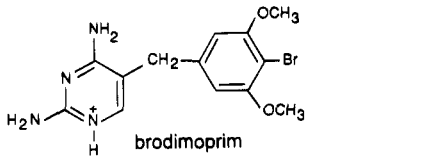

2 brodimoprim

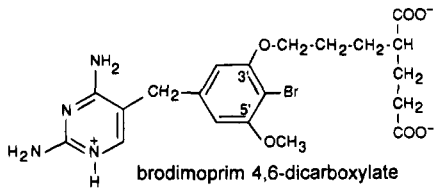

3 brodimoprim 4,6-dicarboxylate

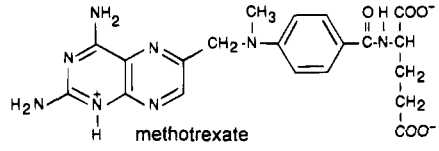

4 methotrexate

Advances in NMR technology and methodology since these earlier studies offer the possibility of obtaining more detailed structural information for complexes formed with proteins of the size of dihydrofolate reductase (molecular weight 18300). In this paper we describe the sequence-specific assignments of the proton resonances in the complex of the brodimoprim-4,6-dicarboxylate analogue with *L. casei* dihydrofolate reductase and compare these with assignments made previously for complexes of trimethoprim (Martorell *et al.*, 1994) and methotrexate (Birdsall *et al.*, 1990; Carr *et al.*, 1991; Soteriou *et al.*, 1993) with the enzyme. Intermolecular and intramolecular proton−proton NOEs between protons on the ligand and on the protein have been measured to provide distance constraints, and these have been used in simulated annealing (Nilges, 1992) and energy minimization calculations to dock the brodimoprim-4,6-dicarboxylate **3** into its binding site in the enzyme and to determine the conformation of the bound ligand and its effects on neighboring residues in the binding site.

MATERIALS AND METHODS

Materials. *L. casei* DHFR was prepared as described previously from an *Escherichia coli* strain into which the structural gene for the *L. casei* enzyme had been cloned (Andrews *et al.*, 1985; Dann *et al.*, 1976). Brodimoprim-4,6-dicarboxylate was prepared as described previously (Kompis & Then, 1984). Solid brodimoprim-4,6-dicarboxylate **3** (1.7−3.0 equiv) was added to the enzyme solution, which was dialyzed in some cases to remove excess ligand and to adjust the salt concentrations. The sample was freeze-dried and made up with D_2O or 90% H_2O/10% D_2O as appropriate for the experiment. The NMR experiments were carried out on an 0.6-mL sample of 4.5 mM DHFR in 500 mM potassium chloride and 50 mM potassium phosphate buffer, pH* 6.5 (pH* values are pH meter readings uncorrected for deuterium isotope effects). The preparation of the trimethoprim−dihydrofolate reductase complex has been described previously (Martorell *et al.*, 1994).

NMR Experiments. The experiments were performed on Varian UNITY 600- and 500-MHz spectrometers with the probe temperature set at 308, 283, and 278 K. The experiments included DQF-COSY (Rance *et al.*, 1983), TOCSY (Bax & Davis, 1985; Braunschweiler & Ernst, 1983) (isotropic mixing times of 40−70 ms), NOESY (Jeener *et al.*, 1979; Macura *et al.*, 1981) (mixing times from 50 to 100 ms), and ROESY (Bothner-By *et al.*, 1984) (mixing times of 35−40 ms). All the spectra were acquired in the phase-senstive mode.

Water suppression was achieved by selective presaturation at the water frequency using either continuous-wave irradiation or a DANTE sequence (Morris & Freeman, 1978). A 180° proton pulse was applied at the center of the mixing time of the NOESY experiments to minimize recovery of the solvent signal and a 60-ms SCUBA sequence was applied immediately after the presaturation period, to allow the restoration of magnetization to the bleached α-CH protons resonating close to the water frequency (Brown *et al.*, 1988).

The spectra from 2D NMR experiments were typically acquired over 1−2 days, by collecting 512−873 t_1 increments, 64−192 scans/increment, and 4096−10 176 points/scan. The spectral width was set at 12.8, 14.0 or 25.4 ppm. The largest spectral width was needed to observe the low-field HN1 signal from bound brodimoprim-4,6-dicarboxylate. Processing of 2D data was carried out by using standard VNMR (Varian) and Felix (Biosym) NMR software. The original data were usually zero-filled once in F_2 and twice in F_1. Resolution enhancement was achieved by applying shifted gaussian apodization functions in both dimensions.

Volume integration of the NOE cross-peaks was performed using the Felix program after applying baseline correction and 90° shifted sine-bell-squared weighting functions. The NOEs were classified as strong (1.8−2.5 Å), medium (1.8−3.0 Å), weak (1.8−4.0 Å), and very weak (1.8−5.0 Å) signals. A correction of 1 Å was added to distance constraints obtained from cross-peaks involving protons in rapidly rotating methyl groups (such as the Met 39 methyl and the ligand 5′-OCH_3 groups). Appropriate corrections were also added in cases where pseudoatom center averaging had to be used (Wüthrich, 1986; Wüthrich *et al.*, 1983). These corrections were not required in some cases where r^{-6} distance averaging could be used.

Molecular Modeling. Heavy-atom coordinates of DHFR were extracted from the X-ray crystallographic data obtained

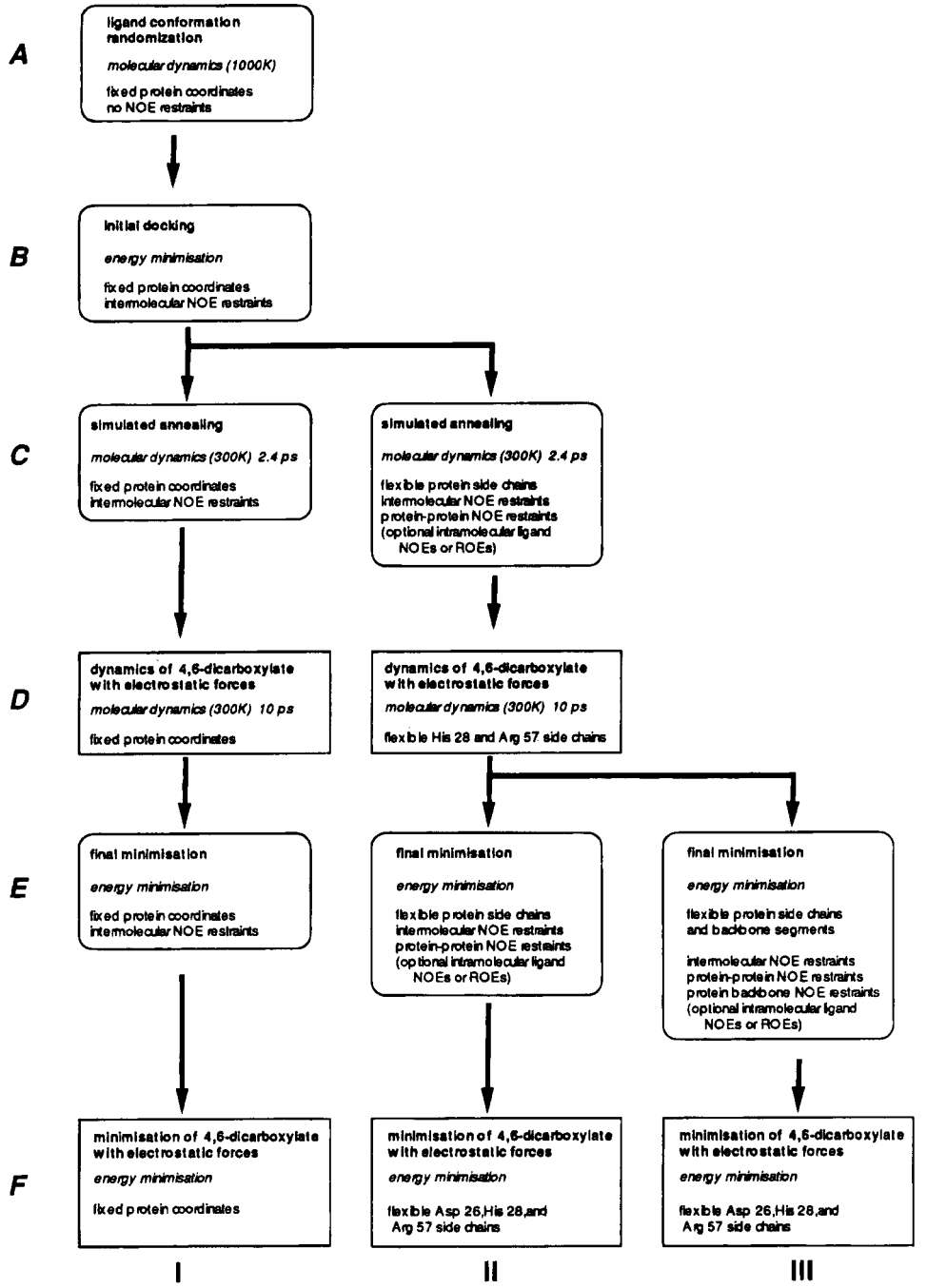

FIGURE 1: Summary of the procedure used for docking the ligand in the inhibitor binding site on DHFR. The three pathways (labeled at the bottom I–III) represent the main variations used [fixed protein coordinates (I), flexible side chains near the binding site (II), and both side-chain and backbone segment flexibility (III)]. The optional phases where electrostatic forces were included in the modeling are shown in rectangles without round corners (D, F).

for the *L. casei* DHFR–methotrexate–NADPH complex (Bolin *et al.*, 1982). The missing side chain of Lys 51 was added in an extended conformation, and corrections of the original sequence data were made to Asp 8, Asp 10, and Pro 90. Structures of the enzyme–ligand complex were calculated, displayed, and manipulated using the Insight II and Discover programs within the Biosym package (Biosym Ltd) on a Silicon Graphics Indigo R4000 Elan/XZ. Hydrogen atoms were added to the heavy atoms of the protein in the Builder module of the Insight II program and then, using Discover, 2500 steps of Powell minimization with a consistent valence force field (CVFF) were performed to remove any bad atom–atom van der Waals contacts. The imidazole rings of the histidine side chains were also protonated. A structure of the ligand, brodimoprim-4,6-dicarboxylate (**3**), was created using the Builder module of Insight II. Partial charges on the ligand were obtained from molecular orbital self-consistent field (MO SCF) calculations using the Biosym MOPAC program with AM1 parametrization (Dewar *et al.*, 1985).

Protocols Used for NMR-Based Docking Calculations. The docking procedure is summarized in the flow chart given in Figure 1. The starting coordinates used for the calculations have the ligand completely outside of the protein (~20 Å away). A nonrestrained molecular dynamics calculation for 1 ps at 1000 K was initially carried out to randomize the conformation of the ligand while the protein coordinates were held fixed (stage A in Figure 1). The initial docking was then performed by an energy minimization procedure using a CVFF force field and with the protein coordinates still held

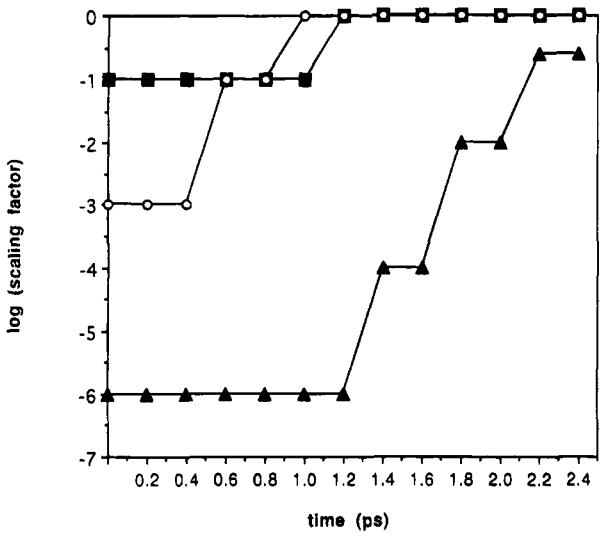

FIGURE 2: Scaling factors used for the torsion angle (■), nonbond (▲), and NOE (○) terms at different times in the trajectory of the restrained molecular dynamics phase in the simulated annealing calculations (stage C in Figure 1).

fixed (stage B). No Morse potentials or cross terms were included in the force field. A quartic nonbond function was used, with a cutoff distance of 8 Å, and the force constants for the NOE distance constraints were set throughout at 20 kcal mol^{-1} $Å^{-1}$. The initial docking was performed in an energy minimization procedure by applying weak forces (0.001−0.1 of the final values) based on NOE constraints. The value of the torsional forces and nonbonded interactions were also set initially at reduced levels to facilitate the docking process. Thus, the first stage of minimization involved 100 cycles of steepest descent minimization with the following scaling factors: torsional forces, 0.1; nonbond interactions, 1.0×10^{-6}; NOE forces, 0.001. The initial docking process was completed by applying 500 cycles of conjugate gradient minimization with the following scaling factors: torsional forces, 0.1; nonbond interactions, 1.0×10^{-6}; NOE forces, 0.1.

The protein−ligand complex was then subjected to restrained molecular dynamics for a total of 2400 steps of 1 fs each at 300 K (stage C), beginning with scaling factors set at 0.1 (torsional forces); 1.0×10^{-6} (nonbond interactions), and 0.001 (NOE forces). During the dynamics phase the scaling factors for the different terms were gradually introduced as indicated in Figure 2: the NOE force scaling factor was increased first to 0.1 (after 0.4 ps) and then to a final value of 1.0 (after 1 ps), the torsional force scaling factor was then increased to 1.0 (after 1.1 ps), and finally, the nonbond interaction scaling factor was gradually increased to a final value of 0.25 (at 2.2 ps). The restrained molecular dynamics were mainly performed in two ways: in one approach, the protein coordinates were kept fixed throughout (column I of Figure 1), and in the second method, flexibility of the side chains (column II) was permitted for those amino acids in contact with the ligand (as indicated by intermolecular NOEs). The relevant side chains were Leu 4, Leu 19, Asp 26, Leu 27, Tyr 29, Phe 30, Phe 49, Leu 54, and Thr 116. In the second approach, intramolecular protein NOE constraints were used in addition to intermolecular protein−ligand NOE constraints. Intramolecular ligand NOEs were also included in some cases. Following this molecular dynamics phase, a final energy minimization of the docked complex was performed with the scaling factors for nonbond interactions, NOE constraints, and torsional forces all set at their final values of 1.0 (stage E). A 6−12 Lennard-Jones potential was used for the nonbond interactions. Minimization was performed for 100 cycles using steepest descents, followed by 2000 cycles using conjugate gradients to convergence with a maximum derivative of 0.002 kcal mol^{-1} $Å^{-1}$. In the case where backbone flexibility was introduced (column III), flexibility was permitted for both the backbone and side chains, for residues in the segments Leu 4−Ala 6, Asp 26−Val 35, and Ser 48−Leu 54 (together with side chains of Leu 19 and Thr 116). Additional backbone NOE constraints were applied during the final minimization (see later).

The above calculations were all performed without using terms for electrostatic interactions in the force field. As an alternative option, separate molecular dynamics (stage D) and final minimization (stage F) calculations were carried out in the presence of electrostatic forces (with a distance-dependent dielectric constant). In stage D, the 300 K molecular dynamics phase was followed by minimization (100 cycles, steepest descent; 500 cycles, conjugate gradient) and then by an additional phase of molecular dynamics (300 K, 10 000 steps of 1 fs each) in which all coordinates were fixed except for the side chains of His 28 and Arg 57 and the dicarboxylate side chain of the ligand. The final minimization was then resumed as described above, first without electrostatic forces included (stage E), and then followed by a second minimization which included electrostatic forces (stage F), during which all coordinates except for Asp 26, His 28, Arg 57, and ligand dicarboxylate side chains were fixed (100 cycles, steepest descent; 2000 cycles, conjugate gradients; to 0.002 kcal mol^{-1} $Å^{-1}$ maximum derivative.

RESULTS AND DISCUSSION

Resonance Assignments. The starting point for assigning the resonances of the complex of brodimoprim-4,6-dicarboxylate with *L. casei* DHFR was a comparison of its spectra with those from the closely related complex of trimethoprim with the enzyme. In previous studies on the latter, assignments were obtained for more than 90% of the proton resonances, including signals from most of the residues in the antifolate drug binding site (Martorell *et al.*, 1994). Such detailed assignments were made possible by examining complexes formed with ^{15}N- and $^{15}N/^{13}C$-labeled protein and by using the full range of heteronuclear 3D experiments available (Clore & Gronenborn, 1991). These detailed assignments on related complexes proved very useful in making the assignments for the complex of the brodimoprim analogue formed with the nonlabeled protein. Comparisons of the 2D DQF−COSY and NOESY spectra of the brodimoprim-4,6-dicarboxylate complex with those from the trimethoprim complex showed that the majority of the ^1H signals had the same chemical shifts (within the range ±0.05 ppm) for the two complexes. Most of the signals in the spectra of the brodimoprim-4,6-dicarboxylate complex could thus be assigned simply by identifying the unshifted signals in the spectra of the two complexes. The subsequent spectral analysis concentrated on assigning the clearly shifted peaks. The similarity of parts of the structure of brodimoprim-4,6-dicarboxylate to parts of trimethoprim would suggest that parts of these ligands will have the same binding sites in the enzyme. However, the differences in their structures will also result in some spectral differences. Similar spectral

comparisons were made between the DHFR complexes with brodimoprim-4,6-dicarboxylate and with methotrexate in order to identify the set of resonances whose chemical shifts are influenced differently in the two complexes. Previous X-ray and NMR structural studies had identified the residues in the DHFR binding sites for trimethoprim and methotrexate (Bolin *et al.*, 1982; Baker *et al.*, 1981; Matthews *et al.*, 1985; Hammond *et al.*, 1986). These include residues Leu 4, Trp 5, Ala 6, Leu 19, Ala 97, Thr 116, and residues in the stretches 24−35 and 45−54. Table 1 gives the resonance assignments for protons in residues from these regions.

Backbone Resonance Assignments. These assignments were based on considering the HN−HA cross-peaks detected in the fingerprint region of 2D ^{1}H DQF−COSY, TOCSY and NOESY spectra of the brodimoprim-4,6-dicarboxylate-DHFR−complex. Several resonances had significantly different chemical shifts in the two complexes and these proved to be from protons clustered in two segments, one in helix B (residues 24−35) and the other in helix C and its adjacent loop (residues 48−54), that is, residues that are either in or near the ligand binding site. Most of these signals were identified by using TOCSY and NOESY connections between their side chain proton resonances and by the standard procedures for sequential assignments based on detecting NOE connections between protons in neighboring residues in the sequence. All the identifiable signals from residues outside the above segments showed no chemical shift differences between the spectra of the brodimoprim-4,6-dicarboxylate and trimethoprim complexes with DHFR. This includes most of the residues in the stretches 1−3, 7−18, 36−47 and 60−162, suggesting that there are no major structural changes in the backbone of the main-chain residues in these regions.

Side-Chain Resonance Assignments. Cross-peaks involving the side-chain proton resonances in the DQF-COSY and TOCSY spectra also showed relatively few differences between the brodimoprim-4,6-dicarboxylate and trimethoprim complexes with the enzyme (spectra not shown). Tyr 29, Phe 30 and Phe 49 are the only aromatic residues with side-chain protons which exhibited chemical shift differences (>0.05 ppm). Relatively few differences were found for the signals from side-chain protons of aliphatic residues (differences were seen only in one of 16 Val residues, one of 14 Thr residues, and five of the 13 Leu residues). The signals which showed differences were assigned by the TOCSY and NOESY connections to the NH and Hα resonances and by their NOESY connections to protons in neighboring residues in the sequence. Further analysis of the shifted signals showed that, once again, they were clustered in residues expected to be in contact with the ligand or in the proximity of the binding site. In fact, many of the protons with shifted signals are involved in intermolecular NOEs with ligand protons (see later).

All the signals with chemical shift differences greater than 0.05 ppm between the brodimoprim-4,6-dicarboxylate and trimethoprim complexes are included in Table 1, together with the chemical shift differences from the corresponding signals in the methotrexate−DHFR complex. The protein protons showing chemical shift differences between the brodimoprim-4,6-dicarboxylate and methotrexate complexes with DHFR are only found in residues expected to be in the vicinity of the ligand binding site. This confirms that the overall structure of the enzyme is similar in all three complexes considered here.

Identification of Bound Ligand Signals. Resonance assignments for the protons of the brodimoprim 4,6-dicarboxylate ligand bound to DHFR are listed in Table 2. The inhibitor can be divided structurally into three moieties, the 2,4-diaminopyrimidine ring (DAP), the benzyl ring, and the 4,6-dicarboxylate side chain (see **3**).

The DAP ring and the C7 methylene bridge are identical to those in TMP and can be shown to be in a very similar binding site environment. The proton resonances for the DAP ring in TMP bound to DHFR have previously been assigned (Martorell *et al.*, 1994), and it proved relatively straightforward to make the corresponding assignments for the brodimoprim-4,6-dicarboxylate complex. The patterns of NOESY cross-peaks observed for the DAP protons in bound brodimoprim-4,6-dicarboxylate (data not shown) are very similar to those for TMP, with only minor chemical shift differences, and all the signals could easily be identified by comparing spectra of the two complexes. Three of the signals, the HN1 of the protonated DAP ring and the HN2A and HN2B protons of the 2-amino group, give well-resolved signals at low field, as was also observed for bound TMP. Strong NOESY cross-peaks with characteristically large line widths were seen between the HN2A and HN2B protons and also between the HN4A and HN4B protons of the 4-amino group, identifying the two pairs of amino proton signals. The H6 proton of the DAP ring has an identical chemical shift in both complexes and its characteristically sharp signal could be positively identified by the very intense NOESY cross-peak to the HN1 signal. The signals assigned to HN1 and the 2- and 4-amino group NH protons were absent in spectra recorded on samples in D_2O.

It was much more difficult to make the resonance assignments for the protons in the benzyl ring. The corresponding signals have not been completely characterized in the spectra of the TMP complex with DHFR (Martorell *et al.*, 1994). Substitution of a Br atom for the OCH_3 group is not in itself expected to cause a large shielding change in the other ring protons (Emsley *et al.*, 1966). However, the benzyl ring might bind differently in the two complexes and this could give different bound chemical shifts. Following detailed comparison of the spectra for the complexes, it was possible to identify a TOCSY peak involving a proton signal in the aromatic region that did not correspond to any expected protein signal. This peak is present only in the spectrum of the brodimoprim-4,6-dicarboxylate complex and has been identified as the cross-peak between H2′ and H6′. These protons do not give separate signals in the case of the TMP−DHFR complex at this temperature (308 K) but give a very broad averaged signal because of intermediate rates of ring flipping (Martorell *et al.*, 1984). However, in subsequent experiments on the TMP−DHFR complex at a lower temperature (≤278K), the ring-flipping rate was found to be sufficiently reduced to allow separate signals for the H2′ and H6′ of TMP to be observed in NOESY and ROESY (Table 2). The chemical shifts of the proposed H2′ and H6′ signals from the brodimoprim-4,6-dicarboxylate−DHFR complex are in good agreement with the values observed for these protons in the TMP complex (Table 2).

Sections of the NOESY spectrum containing the brodimoprim-4,6-dicarboxylate intramolecular NOE cross-peaks are shown in Figure 3. Starting from the H2′ and H6′ resonances of bound brodimoprim-4,6-dicarboxylate, it was possible to identify a pattern of strong and unusually sharp NOE cross-peaks to several proton signals in the NOESY

Table 1: Resonance Assignments and Chemical Shift Comparisons for Binary Complexes of DHFR with Brodimoprim-4,6-dicarboxylate, Trimethoprim, and Methotrexate

residue	proton	chemical shift[a] BDM-4,6	shift difference from TMP[b]	shift difference from MTX[c]	residue	proton	chemical shift[a] BDM-4,6	shift difference from TMP[b]	shift difference from MTX[c]
Leu 4	HN	8.84	nc [d]	nc	Gln 33	Hβ1,Hβ2	1.36	nc	nc
Leu 4	Hα	6.21	nc	nc	Gln 33	Hγ1	1.97	nc	0.52
Leu 4	Hβ1	1.99	−0.07	−0.06	Gln 33	Hγ2	1.97	nc	0.62
Leu 4	Hβ2	1.35	−0.06	nc	Gln 33	Hδ1	5.83	nc	nc
Leu 4	Hγ	2.32	nc	nc	Gln 33	Hδ2	6.55	nc	nc
Leu 4	Hδ1	1.16	nc	nc	Thr 34	HN	7.34	0.18	nc
Leu 4	Hδ2	0.52	−0.13	nc	Thr 34	Hα	4.17	nc	nc
Trp 5	HN	9.28	nc	nc	Thr 34	Hβ	3.81	0.19	0.10
Trp 5	Hα	5.50	nc	nc	Thr 34	Hγ1	3.93	0.14	0.10
Ala 6	HN	8.62	nc	nc	Thr 34	Hγ2	0.22	−0.14	nc
Ala 6	Hα	5.38	nc	nc	Val 35	HN	7.95	0.36	−0.15
Ala 6	Hβ	1.42	nc	nc	Val 35	Hα	3.84	0.15	nc
Leu 19	HN,Hα	na			Val 35	Hβ	2.05	0.07	−0.07
Leu 19	Hβ	na			Val 35	Hγ1,Hγ2	0.99	nc	nc
Leu 19	Hγ	1.26	−0.07	−0.14	Thr 45	HN	7.77	nc	−0.07
Leu 19	Hδ1	0.67	nc	nc	Thr 45	Hα	3.42	nc	−0.31
Leu 19	Hδ2	0.37	nc	−0.08	Thr 45	Hβ	3.91	nc	−0.13
Trp 21	HN	5.64	nc	−0.14	Thr 45	Hγ2	0.67	nc	−0.44
Trp 21	Hα	4.63	nc	−0.08	Tyr 46	HN	7.91	−0.12	−0.35
Trp 21	Hϵ	10.16	nc	0.44	Tyr 46	Hα	3.75	0.55	0.89
Trp 21	Hδ1	6.38	nc	−0.10	Tyr 46	Hβ1	2.77	−0.06	nc
Trp 21	Hϵ3	6.14	nc	0.11	Glu 47	HN	8.02	nc	nc
Trp 21	Hζ3	6.62	nc	0.06	Glu 47	Hα	3.58	nc	nc
Trp 21	Hη2	7.44	nc	0.11	Ser 48	HN	7.33	nc	−0.11
Trp 21	Hζ2	7.03	nc	nc	Ser 48	Hα	4.33	0.06	nc
Leu 23	HN	8.76	nc	−0.37	Ser 48	Hβ1	3.96	0.17	−0.10
Leu 23	Hα	4.78	nc	nc	Ser 48	Hβ2	4.03	0.10	0.13
Leu 23	Hβ1	2.03	nc	0.22	Phe 49	HN	7.05	nc	−0.13
Leu 23	Hβ2	1.04	nc	nc	Phe 49	Hα	4.98	0.09	0.54
Leu 23	Hγ	1.00	nc	nc	Phe 49	Hβ1	2.92	nc	0.13
Leu 23	Hδ1	0.70	nc	nc	Phe 49	Hβ2	2.90	nc	0.11
Leu 23	Hδ2	−0.02	0.06	−0.08	Phe 49	Hδ	6.79	nc	0.41
Asp 25	HN	na			Phe 49	Hϵ	6.40	−0.07	−0.66
Asp 25	Hα	4.31	nc	nc	Phe 49	Hζ	6.88	nc	−0.29
Asp 25	Hβ1	3.07	nc	nc	Pro 50	all	na		
Asp 25	Hβ2	2.30	nc	nc	Lys 51	HN	6.89	−0.29	nc
Asp 26	HN	6.87	−0.11	−0.10	Lys 51	Hα	4.31	nc	nc
Asp 26	Hα	5.26	nc	−0.11	Arg 52	HN	7.97	−0.14	nc
Asp 26	Hβ1	2.61	nc	0.09	Arg 52	Hα	4.36	nc	nc
Asp 26	Hβ2	2.25	nc	nc	Arg 52	Hδ	2.69	nc	nc
Leu 27	HN	7.27	−0.20	−0.13	Arg 52	Hϵ	6.84	nc	0.13
Leu 27	Hα	4.22	nc	0.32	Pro 53	all	na		
Leu 27	Hβ1	2.00	nc	0.18	Leu 54	HN	9.49	nc	0.30
Leu 27	Hβ2	0.95	nc	−0.14	Leu 54	Hα	4.39	−0.09	nc
Leu 27	Hγ	1.66	−0.07	0.21	Leu 54	Hβ1	1.42	−0.07	0.14
Leu 27	Hδ1	0.95	nc	0.31	Leu 54	Hβ2	1.07	nc	0.14
Leu 27	Hδ2	0.54	−0.08	0.55	Leu 54	Hγ	1.51	0.20	0.36
His 28	HN	8.14	−0.10	0.29	Leu 54	Hδ1	0.06	−0.19	0.13
His 28	Hα	4.52	nc	−0.15	Leu 54	Hδ2	0.58	nc	0.23
His 28	Hβ1	3.38	nc	nc	Pro 55	Hα	4.53	nc	nc
His 28	Hβ2	3.49	nc	nc	Pro 55	Hβ1	2.44	nc	nc
His 28	Hδ2	7.45	0.39	0.06	Pro 55	Hβ2	2.05	nc	nc
His 28	Hϵ1	8.46	0.59	nc	Pro 55	Hγ	na		
Tyr 29	HN	8.11	−0.08	0.16	Pro 55	Hδ	na		
Tyr 29	Hα	4.20	nc	nc	Glu 56	HN	9.13	nc	nc
Tyr 29	Hβ1	3.39	nc	nc	Glu 56	Hα	3.91	nc	nc
Tyr 29	Hβ2	3.06	−0.07	nc	Arg 57	HN	7.73	nc	nc
Tyr 29	Hδ	6.78	nc	nc	Arg 57	Hα	4.67	nc	nc
Tyr 29	Hϵ	6.62	nc	nc	Arg 57	Hβ,γ	na		
Phe 30	HN	9.34	nc	0.18	Arg 57	Hδ1	3.02	nc	nc
Phe 30	Hα	3.64	nc	0.06	Arg 57	Hδ2	2.58	nc	nc
Phe 30	Hβ1	3.16	−0.27	nc	Arg 57	Hϵ	6.01	nc	0.33
Phe 30	Hβ2	2.97	nc	nc	Asn 59	HN	9.65	nc	nc
Phe 30	Hδ	6.89	0.11	0.14	Asn 59	Hα	5.00	nc	nc
Phe 30	Hϵ	7.03	−0.06	−0.10	Asn 59	Hβ1	3.10	nc	0.81
Phe 30	Hζ	7.32	nc	−0.06	Asn 59	Hβ2	2.23	nc	−0.92
Arg 31	HN	8.30	0.47	0.12	Asn 59	Hδ1	7.83	0.09	nc
Arg 31	Hα,side	na			Asn 59	Hδ2	6.89	−0.06	nc
Ala 32	HN	7.73	−0.12	−0.11	Ala 97	HN	9.25	nc	nc
Ala 32	Hα	3.93	nc	nc	Ala 97	Hα	5.88	nc	−0.10
Ala 32	Hβ	1.37	nc	nc	Thr 116	Hα	4.83	nc	−0.07
Gln 33	HN	7.94	nc	nc	Thr 116	Hγ1	5.13	nc	0.16
Gln 33	Hα	4.07	nc	nc					

[a] Measured in parts per million and referenced to DSS, at 308 K. [b] TMP−DHFR complex (Martorell *et al.* 1994). Values listed are the TMP chemical shifts subtracted from the brodimoprim-4,6-dicarboxylate chemical shifts. [c] MTX−DHFR complex (Carr *et al.* 1991; Soteriou *et al.*, 1993). Values listed are the MTX chemical shifts subtracted from the brodimoprim-4,6-dicarboxylate chemical shifts. [d] nc, no chemical shift difference (≤0.05 ppm). [e] na, not assigned.

Table 2: ^{1}H Resonance Assignments of Brodimoprim-4,6-dicarboxylate and Trimethoprim Bound to DHFR[a]

atom	4,6-BDM	TMP[b]
HN1	14.99	14.85
HN2A	10.53	10.46
HN2B	5.90	5.90
HN4A	9.41	9.18
HN4B	7.32	7.18
H6	6.51	6.52
H7A	3.89	3.74
H7B	3.49	3.22
H2′	5.05	5.86[c] (4.97[d])
H6′	6.93	5.86[c] (6.81[d])
5′-OCH_3	3.98	(3.83[d])
4′-OCH_3		3.84
3′-OCH_3		(3.42[d])
3′-OCH_2 (H1A)	2.87	
3′-OCH_2 (H1B)	3.04	

[a] Measured in parts per million and referenced to DSS. [b] Martorell *et al.*, 1994. [c] Averaged signal at 308 K. [d] Measured at 278 K.

spectrum of the complex including those from the H7A and H7B protons of the methylene bridge. The latter could be assigned by examining the TOCSY spectrum where there is a cross-peak between the H7A and H7B signals as well as weaker cross-peaks to the DAP ring H6 and benzyl ring H6′. In the NOESY spectrum, H7A and H7B also show very strong NOE cross-peaks to the H6′ proton (Figure 3a) and the HN4A proton (data not shown), as well as less intense cross-peaks to the H2′ and DAP ring H6 signals. The 6′-proton also shows a NOESY cross-peak to a narrow signal at 3.98 ppm which can be assigned to the 5′-OCH_3 protons that resonate at 3.83 ppm in bound trimethoprim. Two other resonances that exhibited very strong NOE cross-peaks to the H2′ proton (Figure 3b) were subsequently found to be connected to each other by a TOCSY cross-peak and were identified as H1A and H1B of the first methylene group of the 4,6-dicarboxylate side chain (corresponding structurally to protons of the 3′-OCH_3 group of TMP). These H1A and H1B signals also have several NOE connections to protons in various protein residues in the benzyl ring binding site, as reported in Table 3A.

It was not possible to extend the ligand signal assignments beyond the first methylene group of the 4,6-dicarboxylate side chain, because of the severe signal overlap in the aliphatic region of the spectra.

Intermolecular and Intramolecular NOEs. The NOE data obtained from the NOESY spectra, as described in the Materials and Methods section, provided the distance constraints listed in Table 3. Figure 4 indicates some of the assigned intermolecular proton−proton cross-peaks in various regions of the NOESY spectrum of the complex. The intermolecular NOEs between the ligand and protein (Table 3A) comprised 19 NOE constraints to the protons on the DAP ring and 19 NOE constraints to the benzyl ring and its substituents (including the first methylene group of the 4,6-dicarboxylate side chain).

Comparison of the listed NOE constraints for the brodimoprim-4,6-dicarboxylate complex with those previously determined for the TMP complex, shows that the protein contacts with the DAP ring protons are broadly similar in both cases. The NOE constraints to the benzyl ring protons are more extensive than for the TMP complex, mainly because of the absence of benzyl ring flipping in the bound brodimoprim-4,6-dicarboxylate. The chemical shift differences between the two inhibitor complexes result in there

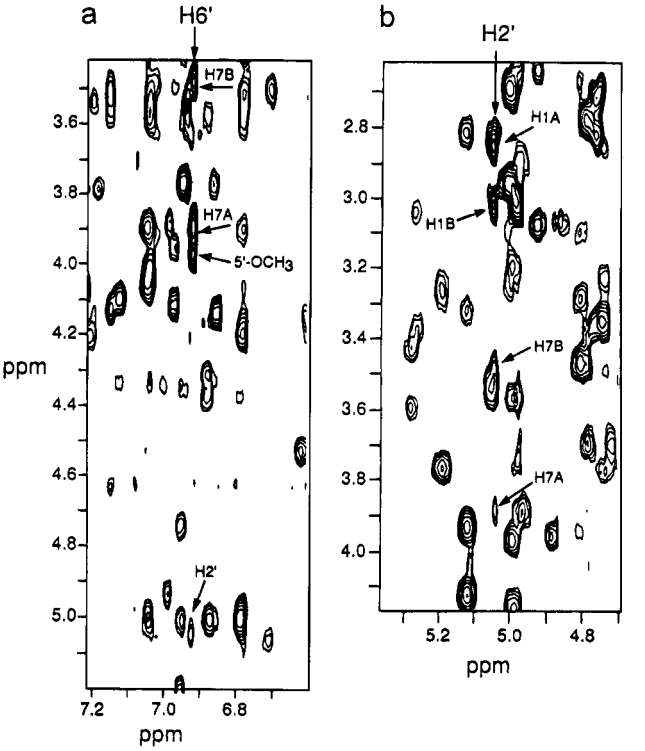

FIGURE 3: Regions of the 2D NOESY spectrum at 600 MHz for the complex of brodimoprim-4,6-dicarboxylate with *L. casei* DHFR showing intramolecular NOEs (a) NOEs from the benzyl 6′ proton; (b) NOEs from the benzyl 2′ proton.

being different cases of degenerate proton chemical shifts in the spectra of the complexes that lead to different ambiguous NOE assignments in the complexes. Thus, a ligand−protein NOE constraint that is present in the list of one complex but absent in that of another does not necessarily imply different binding-site geometries.

In addition to intermolecular NOE constraints, the intramolecular ligand NOE connections listed in Table 3C were also used to help constrain the τ_1 and τ_2 torsion angles that describe the relative conformation of the two ligand rings (**5**).

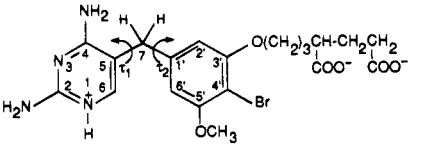

5

Most of these protons are intrinsically close to each other because of the covalent geometry and for this subset of protons, more precise distance constraints were obtained from the NOESY spectra by comparing the cross-peak volumes to reference cross-peaks from protons with a known distance separation (for example, between H2′ and H6′) and by using the r^{-6} relationship. Alternatively, distance restraints for protons near the ligand C7 methylene bridge were derived from ROESY experiments.

An additional set of intramolecular protein NOEs was compiled for the amino acid side chains that were in contact with the ligand (Table 3B). These contacts were used to constrain the ligand binding site residues during the docking procedure described below. In the subsequent calculation, flexibility was permitted for amino acid side chains in the ligand binding site for all amino acids that have protons

Table 3: NOE Constraints Used for Structural Analysis

(A) Intermolecular Ligand−Protein NOEs

ligand proton	protein proton	distance (Å)	strength[a]	ligand proton	protein proton	distance (Å)	strength[a]
HN1	Ala 6 Hβ	1.8−4.0	m	H2′	Phe 49 Hε	1.8−6.4	w
HN1	Thr 116 Hγ1	1.8−5.0	vw	H2′	Phe 49 Hδ	1.8−5.4	m
HN1	Tyr 29 Hδ	1.8−6.4	w	H2′	Phe 30 Hε	1.8−5.4	m
HN1	Phe 30 Hδ	1.8−6.4	w	H2′	Phe 30 Hζ	1.8−6.0	w
HN1	Leu 19 Hδ1	1.8−6.0	vw	H2′	Leu 27 Hδ2	1.8−4.0	m
HN1	Leu 19 Hδ2	1.8−6.0	vw	H6′	Leu 19 Hδ1	1.8−3.5	s
HN1	Asp 26 Hβ	1.8−5.0	w	H6′	Leu 19 Hδ2	1.8−4.0	m
HN1	Leu 27 Hδ2	1.8−5.0	w	H6′	Leu 19 Hγ	1.8−3.0	m
HN1	Phe 30 Hβ	1.8−5.0	w	5′-O-CH_3	Leu 19 Hδ1	1.8−4.5	s
HN1	Thr 116 Hβ	1.8−5.0	vw	5′-O-CH_3	Leu 19 Hδ2	1.8−6.0	w
HN2*	Ala 6 Hβ	1.8−5.0	w	5′-O-CH_3	Leu 19 Hγ	1.8−3.5	m
HN2*	Thr 116 Hγ1	1.8−4.0	w	5′-O-CH_3	Phe 49 Hα	1.8−3.5	s
HN4*	Trp 5 Hα	1.8−4.0	m	5′-O-CH_3	Phe 49 Hε	1.8−6.4	m
HN4*	Ala 6 Hβ	1.8−5.0	m	5′-O-CH_3	Thr 45 Hα	1.8−4.0	m
HN4*	Leu 4 Hγ	1.8−4.0	m	3′-OCH_2 (H1A)	Leu 54 Hδ1	1.8−4.0	m
H6	Leu 19 Hδ1	1.8−3.5	s	3′-OCH_2 (H1A)	Leu 27 Hδ2	1.8−4.0	m
H6	Leu 19 Hδ2	1.8−4.0	m	3′-OCH_2 (H1A)	Phe 49 Hε	1.8−5.4	m
H6	Leu 27 Hα	1.8−4.0	w	3′-OCH_2 (H1B)	Leu 54 Hδ1	1.8−4.0	m
H6	Leu 27 Hγ	1.8−3.0	m	3′-OCH_2 (H1B)	Leu 27 Hδ2	1.8−4.0	m

(B) Brodimoprim-4,6-dicarboxylate Intramolecular NOEs

ligand proton	ligand proton	distance (Å)	strength	ligand proton	ligand proton	distance (Å)	strength
H7A	HN4[b]	1.8−3.13	m	H7A	H2′	1.8−4.24	m
H7B	HN4[b]	1.8−2.69	s	H7B	H2′	1.8−4.24	m
H7A	H6′	1.8−3.47	s	5′-OCH_3	H6′	1.8−4.26	s
H7B	H6′	1.8−3.55	s	3′-OCH_2 (H1A)	H2′	1.8−3.34	s
H7A	H6	1.8−4.5	w	3′-OCH_2 (H1B)	H2′	1.8−3.25	s
H7B	H6	1.8−4.5	w				

(C) Protein NOEs between Side-Chain Protons

side-chain proton	side-chain proton	distance (Å)	strength	side-chain proton	side-chain proton	distance (Å)	strength
Phe 49 Hε	Leu 54 Hδ1	1.8-6.4	m	Arg 57 Hε	Leu 54 Hγ	1.8-3.0	m
Phe 49 Hε	Leu 54 Hδ2	1.8-6.4	m	Arg 57 Hε	Leu 54 Hβ	1.8-4.0	m
Phe 49 Hε	Leu 54 Hγ	1.8-5.4	m	Arg 57 Hε	Val 35 Hα	1.8-4.0	w
Phe 49 Hε	Val 41 Hγ1	1.8-6.4	m	Leu 4 Hδ1	Tyr29 Hε	1.8-6.4	m
Phe 49 Hε	Val 41 Hγ2	1.8-6.4	m	Leu 4 Hδ2	Met39 Hε	1.8-4.5	s
Phe 49 Hε	Thr 45 Hγ2	1.8-6.4	m	Leu 4 Hδ2	Thr34 Hγ2	1.8-4.5	s
Phe 49 Hε	Met 39 Hε	1.8-5.9	s	His 28 Hδ2	Asp25 Hα	1.8-3.0	m
Phe 49 Hδ	Leu 54 Hδ1	1.8-7.4	w	Asp26 Hβ1	Leu 23 Hδ2	1.8-4.0	m
Phe 49 Hδ	Leu 54 Hγ	1.8-4.9	s	Asp26 Hβ2	Leu 23 Hδ2	1.8-4.0	m
Phe 49 Hδ	Val 41 Hγ2	1.8-5.9	s	Asp26 Hβ1	Leu 27 HN	1.8-4.0	w
Phe 49 Hζ	Met 39 Hε	1.8-5.5	s	Asp26 Hβ2	Leu 27 HN	1.8-4.0	w
Phe 30 Hε	Leu 54 Hδ1	1.8-6.4	m	Tyr 29 Hβ	Phe 30 HN	1.8-4.0	m
Phe 30 Hε	Thr 34 Hγ2	1.8-6.4	m	Tyr 29 Hδ	Phe 30 HN	1.8-5.4	m
Phe 30 Hε	Ala 97 Hβ	1.8-5.9	s	Tyr 29 Hδ	Gln 33 Hγ1,Hγ2	1.8-5.4	m
Phe 30 Hδ	Leu 54 Hδ1	1.8-6.4	m	Leu 54 Hδ2	Met 39 Hε	1.8-5.0	m
Phe 30 Hζ	Leu 54 Hδ1	1.8-7.0	w	Leu 54 Hγ	Met 39 Hε	1.8-4.0	m
Phe 30 Hζ	Ala 97 Hβ	1.8-5.5	s	Thr 116 Hγ2	His 153 Hδ2	1.8-5.5	m
Leu 19 Hδ2	Trp 21 Hε1	1.8-5.0	w	Thr 116 Hγ2	Tyr 155 Hδ	1.8-5.9	s
Leu 19 Hδ2	Leu 27 Hδ1	1.8-5.0	m	Thr 116 Hγ2	Thr 116 Hγ1	1.8-3.5	s
Leu 19 Hδ1	Leu 27 Hδ1	1.8-4.5	s	Thr 116 Hβ	Thr 116 Hγ1	1.8-3.0	m
Leu 19 Hδ1	Trp 21 Hδ1	1.8-5.0	w				

(D) Protein NOEs Involving Backbone Protons

backbone proton	proton	distance (Å)	strength	backbone proton	proton	distance (Å)	strength
Asp 26 HN	Leu 27 HN	1.8−2.9	s	Thr 34 HN	Val 35 HN	1.8−2.9	s
Leu 27 HN	His 28 HN	1.8−2.9	s	Asp 26 Hα	Tyr 29 HN	1.8−3.0	m
His 28 HN	Tyr 29 HN	1.8−2.9	*c*	Asp 26 Hα	Tyr 155 Hε	1.8−5.4	m
Tyr 29 HN	Phe 30 HN	1.8−2.9	s	Leu 27 Hα	Phe 30 HN	1.8−3.0	m
Phe 30 HN	Arg 31 HN	1.8−2.9	s	Tyr 29 Hα	Ala 32 HN	1.8−3.0	m
Arg 31 HN	Ala 32 HN	1.8−2.9	s	Tyr 29 Hα	Ala 32 Hβ	1.8−3.5	m
Ala 32 HN	Gln 33 HN	1.8−2.9	s	Ala 32 Hα	Val 35 Hα	1.8−3.0	m
Gln 33 HN	Thr 34 HN	1.8−2.9	s	Val 35 Hα	Gly 36 HN	1.8−3.0	w

[a] NOE strength defined in Materials and Methods: s, strong; m, medium; w, weak; vw, very weak. [b] HN4A and HN4B undergo exchange, which results in their NOEs being averaged. [c] On diagonal.

showing NOE contacts to the ligand or that are expected to have electrostatic interactions with the ligand. Approximately 40 intramolecular NOEs for the amino acids in this group (Leu 4, Leu 19, Asp 26, Leu 27, His 28, Tyr 29, Phe 30, Phe 49, Leu 54, Arg 57, and Thr 116) were identified. Taken together with the 38 intermolecular NOE contacts from the protein to ligand, this results in approximately 8 NOEs/residue. Finally, additional backbone structural constraints for the helix B segment were also derived (Table 3D).

Comparison with the TMP−DHFR and MTX−DHFR Complexes. Consideration of the resonance assignments for

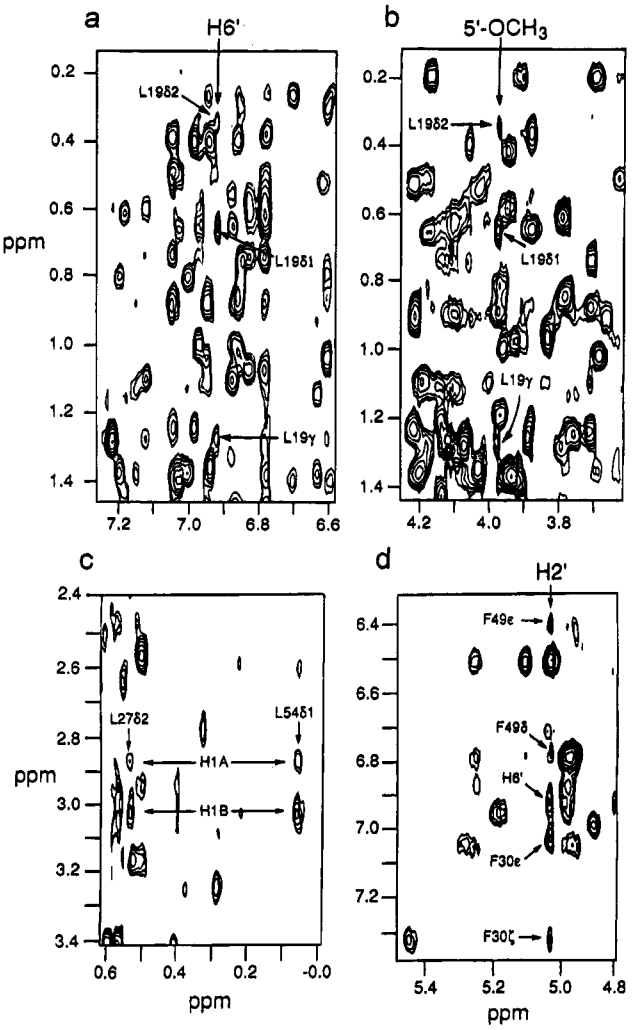

FIGURE 4: Regions of the 2D NOESY at 600 MHz for the complex of brodimoprim-4,6-dicarboxylate showing intermolecular NOEs between protons on the ligand and protein, showing examples of NOEs involving the benzyl ring signals. (a) NOEs from the benzyl ring 6′ protons; (b) NOEs from the 5′-OCH_3 proton; (c) NOEs from the 3′-OCH_2R protons, H1A and H1B; (d) NOEs from the benzyl ring 2′ proton.

the DHFR complexes with the ligands methotrexate, trimethoprim, and brodimoprim-4,6-dicarboxylate has indicated that 90% of the signals have chemical shift differences between the complexes which are less than 0.1 ppm, with most of the chemical shifts agreeing to better than 0.05 ppm. The signals which show differences are from residues near the expected binding site. The NOESY spectra show similar patterns for the vast majority of cross-peaks. Furthermore, the nonexchangeable NH protons and the observed secondary structure elements in all three complexes are the same. These results indicate that the overall conformation of the protein is similar in the different complexes. The NMR data for the binary methotrexate complex of DHFR has already been used to show that the structure is similar to the X-ray structure of the methotrexate−NADPH−DHFR complex (Birdsall *et al.*, 1990; Carr *et al.*, 1991; Soteriou *et al*, 1993). On the basis of these findings, it is reasonable to use the X-ray structure as a starting point for docking experiments with the brodimoprim analogue.

Structure Calculations. In the simplest protocol used in the structure calculations, the protein coordinates were kept fixed throughout the docking procedure. In other simulations, amino acid side chains in contact with the ligand during the docking procedure were allowed to be flexible, and additional relaxation of the binding-site region was allowed during the final minimization in order to optimize side-chain positions and allow backbone adjustments. The different types of NOE constraints given in Table 3 were applied for these purposes as appropriate. In other calculations, flexibility was also allowed in some regions of the backbone (see Materials and Methods section). A further variation in the procedure was to introduce electrostatic forces into the calculations. The possible interactions of the dicarboxylate side chain are not well constrained by experimental NOEs, and these interactions have been modeled by additional dynamics and minimization phases in the presence of electrostatic forces.

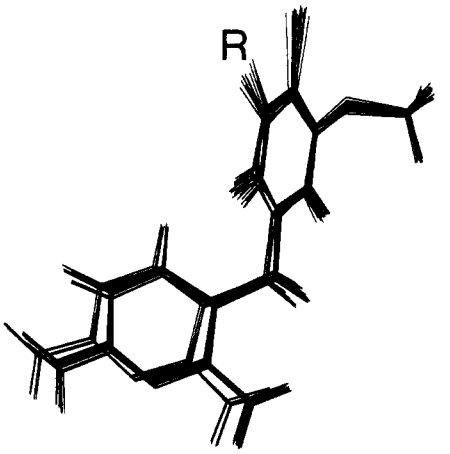

FIGURE 5: Superposition of 20 calculated structures for bound brodimoprim-4,6-dicarboxylate in its complex with *L. casei* DHFR obtained from the simulated annealing and energy minimization procedures outlined in Figure 1. The position of the 4,6-dicarboxylate side chain beyond the oxygen atom is indicated by R on the structure. The structures shown were obtained with flexible side chain and backbone segments, including optional phases with electrostatic forces, and with intramolecular NOE data for the ligand. This corresponds to the flowchart pathway stages (A−F), column III of Figure 1.

Conformation of the Bound Ligand and Structure of the Binding Site: (A) Conformation of the Bound Ligand. Simulations performed with the various protocols gave very consistent results for the bound conformation of the ligand and its position in the binding site. Figure 5 shows the bound ligand conformations calculated using the flexible fitting procedure, where the side chains of the binding-site residues (residues 4, 19, 26, 27, 29, 30, 49, 54, and 116) as well as segments of the backbone were permitted to move under the restraints listed in Table 3A,C,D. The mean torsion angles obtained ($\tau_1 = -153° \pm 4°$, $\tau_2 = 53° \pm 4°$) (see Table 4) were identical to those obtained from the calculations using fixed protein coordinates. However, the extent of ligand−protein NOE violations was significantly greater when the fixed coordinates were used. The fixed protein case typically showed approximately 4 violations in the range 0.3−1.5 Å, while the flexible case had no violations greater than 0.36 Å. Furthermore, the fixed protein structure showed several significant violations of the protein−protein NOE constraints (Table 3C). These involve the side chains of Leu 4, Leu 27, Phe 49, and Leu 54, corresponding mainly to residues in contact with the benzyl ring and the 4,6-dicarboxylate side chain. These violations were all relieved by the flexible fitting procedure. Both procedures docked the DAP ring precisely, but the RMSDs for the benzyl ring of docked structures were substantially lower for flexible fitting pro-

Table 4: Torsion Angles from the Calculated Structures of the Brodimoprim-4,6-dicarboxylate•DHFR Complex

	fixed protein coordinates (IF)[a]	flexible protein (IIIF)[a]
	Ligand Torsion Angles (deg)	
τ_1[b]	−156 ± 3	−153 ± 4
τ_2[b]	51 ± 4	53 ± 4
	RMSD Values[c] (Å)	
DAP	0.40	0.50
benzyl ring	4.27	0.76
	Protein χ_1 Angles (deg)	
Leu 4	173	154
Leu 19	−56	−73
Asp 26	168	−177
Leu 27	−66	−77
Tyr 29	174	168
Phe 30	180	−170
Phe 49	−56	−69
Leu 54	−76	47
Thr 116	−58	−55

[a] Ligand docking procedure, Figure 1. [b] The two torsion angles were defined by the atoms C4−C5−C7−C1′ (τ_1) and C5−C7−C1′-C2′ (τ_2) (**5**); the torsion angles are zero when atoms $\alpha-\beta-\gamma-\delta$ are *syn*-planar, and a positive rotation is one that moves atom δ in a clockwise sense when one looks along the $\beta-\gamma$ bond from β to γ. [c] Rigid body fit of 18 structures to common frame using the molecular similarity module of Quanta (Molecular Simulations Inc.) to superimpose all non-hydrogen atoms of the DAP and/or benzyl rings.

cedures than for procedures using fixed protein coordinates (Table 4). A representative view of the calculated binding site is shown in Figure 6.

In addition to the above constraints, the intramolecular ligand NOE data involving the C7 methylene protons was also used to improve the determination of the conformation of the bound ligand. Similar results for the structure (Table 4) were obtained in the presence or absence of these additional NOE-based distance restraints (Table 3B), indicating that the generated conformations are consistent with both the intramolecular and intermolecular data.

As an alternative procedure, the intramolecular ligand NOE data were used in conjunction with the conformational grid search program AngleSearch to define the conformation of the bound ligand (Polshakov *et al.*, 1985). For one set of assignments for the prochiral C7 methylene protons, permissible torsion angle ranges consistent with the NOE data in Table 3B were determined by AngleSearch to be −141° to −183° for τ_1 and −3° to 60° for τ_2: the alternative set of assignments for the prochiral C7 methylene protons gave 141° to 183° for τ_1 and −60° to 3° for τ_2. The former values are in good agreement with the conformations generated in the restrained molecular dynamics simulations, while the latter torsion angles are not structurally compatible with the enzyme binding site. This approach not only provided information about the conformation of the bound ligand but also gave the stereospecific assignment of the C7 methylene hydrogen atoms within the binding site. Additional ROE data (not given) also confirmed these stereospecific assignments.

(B) Residues in Contact with the Bound Ligand. In general, the conformations of the residues in contact with the DAP ring appear quite similar to those in contact with the corresponding part of the pteridine ring in the crystal structure of the MTX−NADPH−DHFR complex (Bolin *et al.*, 1982), but there were small positional changes in the coordinates for several of the residues that are in contact with the benzyl ring (Figure 7).

Most of the side-chain positions were relatively well-defined. For example, the side chains of Leu 4, Leu 19, Tyr 29, and Thr 116 are well-defined in the docked structures and have torsion angles similar to those found in the MTX−NADPH−DHFR crystal structure (Bolin *et al.*, 1982). Although the side chain of Asp 26 is less well-defined by the NOE contacts, the most common conformation observed for this residue in the simulations resembles that observed in the crystal structure ($\chi_1 \approx 180°$ in 75% of structures). In this conformation, the carboxylate group of Asp 26 interacts with both the HN1 proton and the 2-amino group of brodimoprim-4,6-dicarboxylate. The hydroxy group of Thr 116 is also positioned very close to one of the Asp 26 carboxylate δ oxygens. One of the protons of the 4-amino group of the ligand is close to the carbonyl group of Leu 4. In the crystal structure of the MTX−NADPH−DHFR complex, similar interactions are observed between the corresponding groups; for example, between the HN1 and 2-amino groups of the drug with the Asp 26 on the protein and between the 4-amino group of the drug and the carbonyl groups of Leu 4 and Ala 97.

When the positions of the amino acid side chains in the benzyl ring binding subsite were compared with those in the crystal structure of the MTX−NADPH−DHFR complex, larger differences were seen. Substantial differences were observed for the side chains of Leu 27, Phe 30, Phe 49, Leu 54, and Pro 50 (the latter movement requires flexibility of the backbone as well, as discussed below). The two phenylalanine residues showed χ_1 values similar to the crystal structure (Table 4), but the aromatic rings were significantly rotated ($\chi_2 \approx 30°$ different). The different position of Phe 49 alters ring current shielding effects on nearby residues (in particular, on the HN and Hα protons of Tyr 46, which experience large chemical shift differences between the complexes). The conformation of the ligand benzyl ring and the two phenylalanine residues is consistent with energetically favorable aromatic−aromatic interactions among the three rings (Singh & Thornton, 1985; Burley & Petsko, 1985).

The χ_1 value of Leu 54 was estimated to be in the range of +60 ± 15° from the docking calculations (after minimization without electrostatic forces) and from independent considerations of coupling constant and NOE data relating to the αCH and βCH_2 protons (from intensity data in TOCSY and NOESY spectra) using AngleSearch (Polshakov *et al.*, 1995). Conformations in this range of χ_1 were also associated with ligand structures that have the expected (and most energetically favorable) ionic contacts between the 4- and 6-carboxylate groups with Arg 57 and His 28 residues respectively. The rearranged side chains of both Leu 54 and Leu 27 are in contact with the first three methylene groups of the 4,6-dicarboxylate side chain, thus reflecting favorable hydrophobic interactions.

In calculations where backbone flexibility was introduced, structures were obtained with significant backbone movement of the segment of residues 50−54 compared to their positions in the MTX−NADPH−DHFR structure. The observed structural change relieves the initially observed steric hindrance between Pro 50 and the 4′-bromo substituent of the ligand (Figure 7). It is also consistent with the large chemical shift differences observed for the NH and C-α proton resonances of Lys 51 and Arg 52 when compared with their values in the methotrexate−DHFR complex.

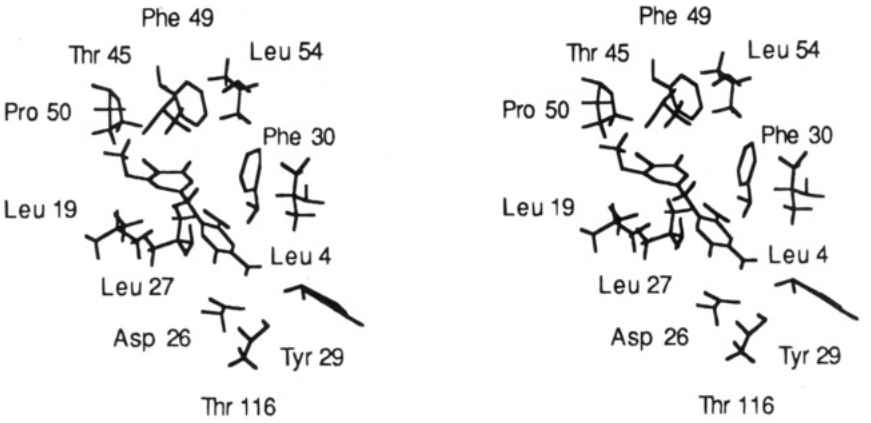

FIGURE 6: Stereoview of a representative calculated structure of brodimoprim-4,6-dicarboxylate, in its binding site and including those protein side chains having protons with intermolecular NOEs to the ligand. Calculations were performed as described in Figure 5.

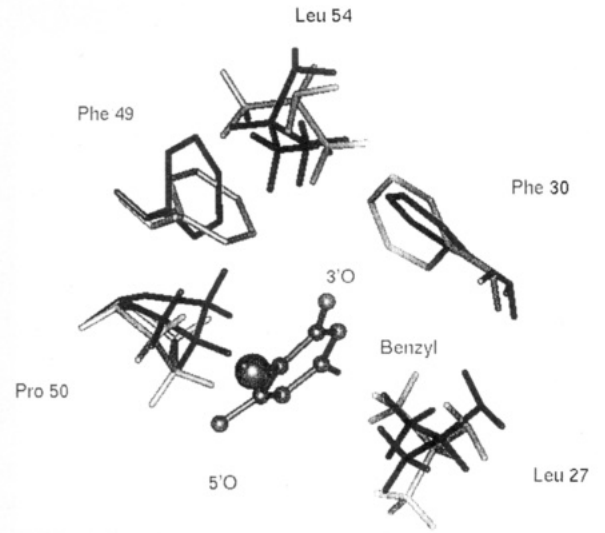

FIGURE 7: Comparison of the positions of the side chains of Leu 27, Phe 30, Phe 49, Pro 50, and Leu 54 in the NMR-determined structure of the brodimoprim-4,6-dicarboxylate complex (light) and the X-ray-determined structure (Bolin *et al.*, 1982) of the complex containing methotrexate (dark). The comparison was made by overlapping the protein backbone atoms in the two structures. Calculations were performed as described in Figure 5.

No substantial structural differences between the complexes were observed for the backbone in helix B (residues 24−34), although there was variability in the surface residues (for example, Arg 31) that were relatively unconstrained by the limited NOE data. The calculated structures for this region had a backbone RMSD of approximately 0.4−0.6 Å compared to the crystal structure backbone.

The final docked structure for the conformation of the ligand and its contact residues was examined for possible binding sites for water. There is space in the structure for a water molecule in contact with the drug HN1 and the Asp 26 carboxylate and also space for another water molecule close to the 2-amino group. These positions would correspond to the water molecules (Wat 253 and Wat 201, respectively) found in contact with methotrexate in the crystal structure (Bolin *et al.*, 1982). In the NMR docked structure the 4-amino group of the ligand does not appear to be close enough to form a direct hydrogen bond with the carbonyl group of Ala 97. However, there is space nearby which could accommodate a water molecule capable of bridging these groups.

(C) Binding of the 4,6-Dicarboxylate Side Chain. In some cases, the final energy minimization was conducted in the presence of electrostatic forces to assist in modeling the 4,6-dicarboxylate chain interactions and conformations as described below. Inclusion of the electrostatic forces in the calculations had no effect on the relative positions of the ligand rings. However, small changes occurred in the position of the Asp 26 side chain, which was slightly closer (by approximately 0.4 Å) to the positively charged ligand HN1 when electrostatic forces were included in the minimization.

The ligand dicarboxylate side chain is not well-constrained by NOEs because of the lack of resonance assignments for protons beyond the first methylene group. However, previous analysis of the NMR spectra and the binding affinities of complexes formed with a series of similar inhibitors indicated that brodimoprim-4,6-dicarboxylate probably forms two ion pairs with cationic residues of the protein (Birdsall *et al.*, 1984b), one of which is His 28. The pK_a value of His 28 has the same value (7.8) in the complexes formed with MTX and with brodimoprim-4,6-dicarboxylate and can be compared with the pK_a value of 6.8 observed for His 28 in the protein in the absence of ligand. This suggests that His 28 is participating in a similar electrostatic interaction with the 4,6-dicarboxylate side chain of the brodimoprim analogue as it does with the γ-carboxylate of the glutamyl moiety of methotrexate (Bolin *et al.*, 1982; Antonjuk *et al.*, 1984). This interaction is probably with the 6-carboxylate group, although interaction with the 4-carboxylate cannot be ruled out. From consideration of the MTX−NADPH−DHFR crystal structure (Bolin *et al.*, 1982), the other ionic interaction with the 4,6-dicarboxylate side chain is expected to involve the Arg 57 guanidinium group although direct NMR evidence for this is lacking.

Possible ion-pair formation of protein residues with the dicarboxylate side chain of brodimoprim-4,6-dicarboxylate was modeled in a second phase of dynamics followed by energy minimization, in the presence of electrostatic forces, with the molecules held fixed in positions determined in the first phase of the calculations except for the 4,6-dicarboxylate and His 28 and Arg 57 side chains. This procedure produced a stochastic distribution of the possible intermolecular ion pairs. The combination of the 6-carboxylate with His 28 and the 4-carboxylate with Arg 57 occurred in 30% of structures and these structures had the minimum energy value, as well as the most favorable average energy, compared with other possibilities. This structure has the same type of interactions as found in the crystal structure of the methotrexate−NADPH−DHFR complex [where the

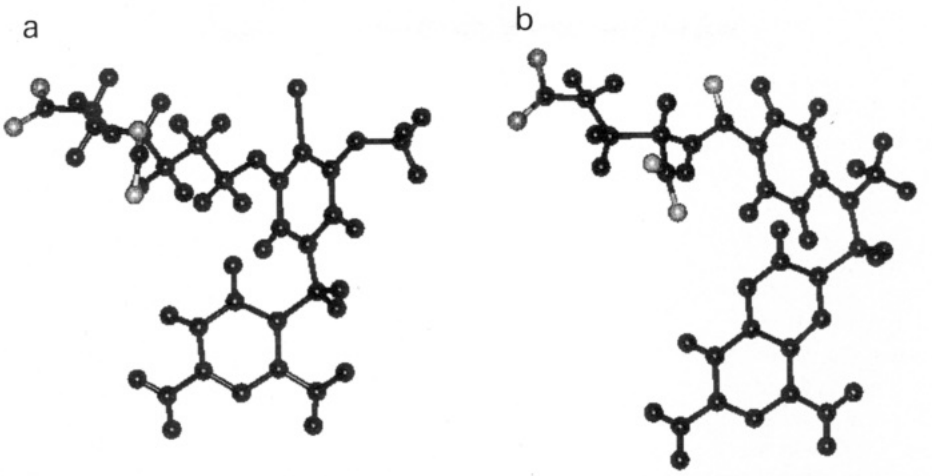

FIGURE 8: Comparable view of the bound ligand conformation of (a) brodimoprim-4,6-dicarboxylate and (b) methotrexate (Bolin *et al.*, 1982). The positions of the protein backbone atoms are the same in the two diagrams (not shown). Calculations were performed as described in Figure 5. The light atoms are the oxygens of the 4,6-dicarboxylate and the glutamate side chains.

glutamyl γ-carboxylate interacts with His 28 and the α-carboxylate interacts with Arg 57 (Bolin *et al.*, 1982)]. Less favorable energy interactions were found in structures involving the reverse combination (the 4-carboxylate with His 28 and the 6-carboxylate with Arg 57) as well as in other structures where only a single electrostatic interaction was present. Energetically less favorable interactions with the Arg 31 and Lys 51 side chains were also seen in a few of the structures.

The conformation of the aromatic rings in the docked ligand determined in the absence of electrostatic interactions was found to be the same as that determined when the electrostatic energy contributions from the ion-pair combinations (6-carboxylate−His 28 and 4-carboxylate−Arg 57) are included. Using the approach described above, the energy calculations indicated that this combination is the most favorable arrangement for the electrostatic interactions.

Despite the fact that the ligand is a racemate (chiral at the 4-carbon of the 4,6-dicarboxylate chain), no doubling of any of the ligand or protein signals was observed. This suggests that one stereoisomer of the ligand binds with much higher affinity than the other, such that one form of the complex predominates. However, one cannot exclude the possibility that the two stereoisomers bind with approximately equal affinities, giving a mixture of two complexes which have the same chemical shifts. The initial docking was performed with the stereoisomer that has a similar configuration to the α-carbon of the glutamyl side chain of MTX (although further modeling with the other stereoisomer indicated that it could also form similar combinations of ion-pair interactions).

(D) Comparisons with Results from Previous Studies. It is interesting to compare the results from this present work with those obtained in earlier studies of the brodimoprim-4,6-dicarboxylate complex formed with dihydrofolate reductase (Birdsall et al., 1984b), which were based on ring-current chemical shift considerations and molecular modeling of the ligand into the fixed protein coordinates from the *L. casei* DHFR−MTX−NADPH X-ray structure (Bolin et al., 1982). The mean τ_1 and τ_2 angles obtained in the present work are in good agreement with those found from the earlier modeling studies ($\tau_1 = -155°$, $\tau_2 = 53°$). It should also be noted that the present τ_1 and τ_2 values are also consistent with those found in a recent NMR study of a trimethoprim−dihydrofolate reductase complex ($\tau_1 = -151° \pm 50°$; $\tau_2 = 43° \pm 37°$).

The similarity in the brodimoprim-4,6-dicarboxylate and trimethoprim ring conformations in their complexes is further supported by the almost identical ^{1}H chemical shifts observed for the H6 proton in the two complexes. The H6 proton is expected to have a large shielding contribution from the benzyl ring (~0.9 ppm) which will depend in a sensitive manner on the relative orientations of the two rings (Birdsall *et al.*, 1984a). The orientations of the two rings must therefore be very similar in the complexes with trimethoprim and the brodimoprim-4,6-dicarboxylate. Thus, the additional interactions made by the 4,6-dicarboxylate side chain with the protein can be made without requiring a change in the conformation of the ligand rings.

It is interesting that the C7 methylene bridge bond angle (C5−C7−C1′) in the bound brodimoprim analogue (118° ± 1°) is quite different from a normal tetrahedral bond angle (109°). A similar C7 methylene bond angle has been reported previously in neutron diffraction studies on trimethoprim crystals (Koetzle & Williams, 1976); this distortion may relieve steric hindrance between the aromatic ring substituents when certain τ_1 and τ_2 angles are imposed by crystal or protein interactions.

Comparisons of the conformation of docked brodimoprim-4,6-dicarboxylate including the expected electrostatic interactions with the His 28 and Arg 57 residues with that of bound methotrexate (Bolin *et al.*, 1982) can also be made. Figure 8 shows the conformations of the two bound ligands in comparable views in the protein (the protein backbone atoms have the same positions in each view). In spite of the structural differences in the two ligands, the overall shape of the ligands is very similar and the two bound structures overlap to a remarkable degree. The somewhat smaller brodimoprim analogue generally fits within the whole boundary of the bound methotrexate. The 5′-OCH_3 group of brodimoprim-4,6-dicarboxylate is close to the position occupied by N-10 CH_3 of bound methotrexate and the 4′-bromo substituent of the brodimoprim analogue is near to two of the *ortho* protons on the methotrexate benzoyl ring. The only notable difference is the first methylene group of the 4,6-dicarboxylate side chain which protrudes outside the boundary of the bound methotrexate.

Conclusions. By using a ligand docking procedure based on NOE distance constraints and allowing for flexibility in the protein residues close to the ligand, it has proved possible to determine the conformation of bound brodimoprim-4,6-dicarboxylate (**3**) and the protein residues near its binding site in dihydrofolate reductase. The asymmetrically substituted benzyl ring of the ligand binds in a single conformation and, unlike trimethoprim, is not involved in ring flipping. This removes problems caused by exchange and makes the analysis of the intermolecular NOEs between the benzyl ring and protein protons straightforward. The conformations of the aromatic rings (defined by τ_1 and τ_2) are similar for bound brodimoprim-4,6-dicarboxylate and trimethoprim. Thus, no conformational adjustment of these rings is required to allow optimal interactions of the 4,6-dicarboxylate groups with the protein residues. This, no doubt, contributes to the large increase in binding affinity of the brodimoprim analogue compared to the parent molecule. However, the side chains of the amino acid residues in contact with the benzyl ring of the ligand (Leu 27, Phe 30, Phe 49, Pro 50, and Leu 54) and the backbone of the loop region containing residues 50–54 show significant differences in conformation when compared to these residues in the benzoyl ring subsite in the crystal structure of the MTX–NADPH–DHFR complex. It is of interest in the context of inhibitor design that flexible side chains and backbone loop regions can adopt different conformations at apparently modest cost to the overall binding energy in order to optimize the hydrophobic interactions with the relevant part of the ligand (benzyl or benzoyl ring) in the two complexes. In contrast, the side-chain interactions with the 2,4-diaminopyrimidine part of the bound ligand, which are mainly electrostatic/hydrogen-bonding interactions, are essentially the same in the two complexes.

ACKNOWLEDGMENT

We thank G. Ostler and J. E. McCormick for expert technical assistance and T. A. Frenkiel and C. J. Bauer for help with some of the NMR experiments. The NMR measurements were made using the facilities at the MRC Biomedical NMR Centre, NIMR, Mill Hill.

REFERENCES

Andrews, J., Clore, G. M., Davies, R. W., Gronenborn, A. M., Gronenborn, B., Kalderon, D., Papadopoulos, P. C., Schafer, S., Sims, P. F. G., & Stancombe, R. (1985) *Gene 35*, 217–222.

Antonjuk, D. J., Birdsall, B., Burgen, A. S. V., Cheung, H. T. A., Clore, G. M., Feeney, J., Gronenborn, A., Roberts, G. C. K., & Tran, W. (1984) *Br. J. Pharmacol. 81*, 309–315.

Baker, D. J., Beddell, C. R., Champness, J. N., Goodford, P. J., Norrington, F. E. A., Smith, D. R., & Stammers, D. K. (1981) *FEBS Lett. 126*, 49–52.

Baker, D. J., Beddell, C. R., Champness, J. N., Goodford, P. J., Norrington, F. E. A., Roth, B., & Stammers, D. K. (1982) in *Chemistry and Biology of Pteridines* (Blair, J. D., Ed.) pp 545–549, W. de Gruyter, Berlin.

Birdsall, B., Griffiths, D. V., Roberts, G. C. K., Feeney, J., & Burgen, A. S. V. (1977) *Proc. R. Soc. London, B 196*, 251–265.

Birdsall, B., Bevan, A. W., Pascual, C., Roberts, G. C. K., Feeney, J., Gronenborn, A., & Clore, G. M. (1984a) *Biochemistry 23*, 4733–4742.

Birdsall, B., Feeney, J., Pascual, C., Roberts, G. C. K., Kompis, I., Then, R. L., Muller, K., & Kroehn, A. (1984b) *J. Med. Chem. 23*, 1672–1676.

Birdsall, B., Arnold, J. R. P., Jimenez-Barbero, J., Frenkiel, T. A., Bauer, C. J., Tendler, S. J. B., Carr, M. D., Thomas, J. A., Roberts, G. C. K., & Feeney, J. (1990) *Eur. J. Biochem. 191*, 659–668.

Blakley, R. L. (1985) Dihydrofolate Reductase, in *Folates and Pterins* (Blakley, R. L., & Benkovic, S. J.. Eds.) Vol. 1, Chapt. 5, pp 191–253, J. Wiley, New York.

Bolin, J. T., Filman, D. J., Matthews, D. A., Hamlin, R. C., & Kraut, J. (1982) *J. Biol. Chem. 257*, 13650–13662.

Bothner-By, A. A., Stephens, R. L., Lee, J., Warren, C. D., & Jeanloz, R. W. (1984) *J. Am. Chem. Soc. 106*, 811–813.

Braunschweiler, L., & Ernst, R. R. (1983) *J. Magn. Reson., 53*, 521–528.

Brown, S. C., Weber, P. L., & Mueller, L. (1988) *J. Magn. Reson. 77*, 166–169.

Burley, S. K., & Petsko, G. A. (1985) *Science 229*, 23–28.

Carr, M. D., Birdsall, B., Jimenez-Barbero, J., Polshakov, V. I., Bauer, C. J., Frenkiel, T. A., Roberts, G. C. K., & Feeney, J. (1991) *Biochemistry 30*, 6330–6341.

Cayley, J., Albrand, J. P., Feeney, J., Roberts, G. C. K., Piper, E. A., & Burgen, A. S. V. (1979) *Biochemistry 18*, 3886–3895.

Clore, G. M., & Gronenborn, A. M. (1991) *Prog. NMR Spectrosc. 23*, 1–41.

Dann, J. G., Ostler, G., Bjur, R. A., King, R. W., Scudder, P., Turner, P. C., Roberts, G. C. K., & Burgen, A. S. V. (1976) *Biochem. J. 157*, 559–571.

Davies, D. G., & Bax, A. (1985) *J. Am. Chem. Soc. 107*, 2820–2821.

Dewar, M. J. S., Zoebisch, E. G., Healy, E. F., & Stewart, J. J. P. (1985) *J. Am. Chem. Soc. 107*, 3902–3909.

Emsley, J. W., Feeney, J., & Sutcliffe, L. H. (1966) *High Resolution Nuclear Magnetic Resonance Spectroscopy*, Vol. 2, p 1140. Pergamon Press, New York.

Feeney, J. (1990) *Biochem. Pharmacol. 40*, 141–152.

Groom, C. R., Thillet, J., North, A. C., Pictet, R., & Geddes, A. J. (1991) *J. Biol. Chem. 266*, 19890–19893.

Hammond, S. J., Birdsall, B., Searle, M. S., Roberts, G. C. K., & Feeney, J. (1986) *J. Mol. Biol. 188*, 81–97.

Jeener, J., Meier, B. H., Bachmann, P., & Ernst, R. R. (1979) *J. Chem. Phys. 71*, 4546–4553.

Koetzle, T. F., & Williams, G. J. B. (1976) *J. Am. Chem. Soc. 98*, 2074–2077.

Kompis, I., & Then, R. L. (1984) *Eur. J. Med. Chem. 19*, 529–534.

Kuyper, L. F., Roth, B., Baccanari, D. P., Ferone, R., Beddell, C. R., Champness, J. N., Stammers, D. K., Dann, J. G., Norrington, F. E. A., Baker, D. J., & Goodford, P. J. (1982) *J. Med. Chem. 25*, 1122.

Macura, S., Huong, Y., Suter, D., & Ernst, R. R. (1981) *J. Magn. Reson. 43*, 259–281.

Martorell, G., Gradwell, M. J., Birdsall, B., Bauer, C. J., Frenkiel, T. A., Cheung, H. T. A., Polshakov, V. I., Kuyper, L., & Feeney, J. (1994) *Biochemistry 33*, 12416–12426.

Matthews, D. A., Bolin, J. T., Burridge, J. M., Filman, D. J., Volz, K. W., Kaufman, B. T., Beddell, C. R., Champness, J. N., Stammers, D. K., & Kraut, J. (1985) *J. Biol. Chem. 260*, 381–399.

Morris, G. A., & Freeman, R. (1978) *J. Magn. Reson. 29*, 433–462.

Nilges, M. (1992) *X*-plor 3.1 manual, pp 316–319, Yale University, New Haven, CT.

Polshakov, V. I., Birdsall, B., Frenkiel, T. A., & Feeney, J. (1995) *J. Magn. Reson. B108*, 31–43.

Rance, M., Sorensen, O. W., Bodenhausen, G., Wagner, G., Ernst, R. R., & Wüthrich, K. (1983) *Biochem. Biophys. Res. Commun. 117*, 479–485.

Roth, B., & Cheng, C. C. (1982) *Prog. Med. Chem. 19*, 1–58.

Singh, J., & Thornton, J. M. (1985) *FEBS Lett. 191*, 1–6.

Soteriou, A., Carr, M. D., Frenkiel, T. A., McCormick, J. E., Bauer, C. J., Sali, D., Birdsall, B., & Feeney, J. (1993) *J. Biomol. NMR 3*, 535–546.

Wüthrich, K. (1986) *NMR of Proteins and Nucleic Acids*, Wiley, New York.

Wüthrich, K., Billeter, M., & Braun, W. (1983) *J. Mol. Biol. 169*, 949–961.

BI950585N